VNU Journal of Science: Mathematics - Physics

Journal homepage: https://js.vnu.edu.vn/MaP

Original Article

Preparation and Characterization of Ultrafine SnO_2 Nanoparticles as Anode Materials in Lithium Ion Batteries

Le Dinh Trong[1,*], Nguyen Van Ky[2], Nguyen Si Hieu[3]

[1]*Hanoi Pedagogical University 2, 32 Nguyen Van Linh, Xuan Hoa, Phuc Yen, Vinh Phuc, Vietnam*

[2]*Le Quy Don Technical University, 236 Hoang Quoc Viet, Bac Tu Liem, Hanoi, Vietnam*

[3]*Institute of Materials Science, Vietnam Academy of Science and Technology, 18 Hoang Quoc Viet, Cau Giay, Hanoi, Vietnam*

Received 10 October 2022
Revised 05 November 2022; Accepted 24 November 2022

Abstract: In this work, ultrafine SnO_2 nanoparticles were prepared by a facile solvothermal route using $SnCl_4.5H_2O$ as initial materials. Phase compositions and microstructures of as-prepared nanoparticles have been investigated by X-ray diffraction (XRD), scanning electron microscopy (SEM), and the particle size analyzer. It was found that the obtained ultrafine SnO_2 nanoparticles with the good dispersibility exhibited a pure rutile structural phase with an average crystal grain size of 7.4 nm. The electrochemical performance was characterized by cyclic voltammetry, galvanostatic cycling, and electrochemical impedance spectroscopy (EIS). The galvanostatic cycling results at a current density of 100 $mAh{\cdot}g^{-1}$ showed that as-prepared SnO_2 nanoparticles possess a high specific discharge capacity of 1379 $mAh{\cdot}g^{-1}$ with a Coulombic efficiency of 57% at the first cycle, this efficiency was over 91% after the 5^{th} cycle, and the specific discharge capacity of 276 $mAh{\cdot}g^{-1}$ was maintained during the 50^{th} cycle of discharge/charge. Despite the relatively low cyclic stability, the effectve electrochemical performance of the SnO_2 electrode due to its ultrafine nanostructure expanded active regions and promoted the reversible process of lithium insertion/extraction.

Keywords: Ultrafine SnO_2 nanoparticles; Solvothermal route; Li-ion battery; Anode material.

1. Introduction

Over the past few decades, rechargeable Li-ion batteries (LIBs) have been used as a common power source in portable electrical and electronic devices, such as mobile phones, laptops, cameras,

* Corresponding author.
E-mail address: ledinhtrong@hpu2.edu.vn

https//doi.org/10.25073/2588-1124/vnumap.4780

camcorders, hand tools, etc., due to their high energy density, low self-discharge, long life cycle, no memory effect, low environmental impact [1, 2]. In the future, Li-ion batteries are still considered as a promising candidate that can be applied to large-power mobile devices such as electric cars, renewable energy storage, and smartly electric grid systems. To live up to expectations, the next-generation Li-ion battery needs to have a higher energy density, a longer life cycle, and a much faster charging rate than those of the current versions [3]. To develop next-generation lithium-ion batteries, new electrode materials and electrolytes are required [4]. The electrode materials are responsible for the transport of charges and energy storage in LIBs, thus being one of the most important components for achieving high energy/power densities, high capacity rates, highly Coulombic efficiency, and cyclic stability [5].

Currently, most commercial LIBs use graphite as the anode electrode material. This is an unsuitable anode material for next-generation LIBs because of its safety concerns and low theoretical capacity of 372 $mAh \cdot g^{-1}$ [5]. In such a context, much research effort has been made to introduce high performance anode electrode materials for LIBs. For more than the past two decades, tin dioxide (SnO_2) has been considered as promising anode electrode materials for LIBs because of its high theoretical capacity (782 $mAh \cdot g^{-1}$ and low discharge potential [5, 6]. In addition, this material is also easy to obtain at low cost, and is eco-friendly [7]. However, SnO_2 has some disadvantages when used as anode electrode material for LIBs: firstly, large capacity loss after the first discharge/charge cycle; secondly, the volume expansion is too large (up to 300%) during the lithiation/de-lithiation process resulting in electrode pulverization and losing electrical contact [8]. Furthermore, the breakdown of primary particles and after that, the agglomeration of the broken particles can lead to a significant reduction in their Li^+ active sites resulting in poor cyclic efficiency, fast capacity decay and low Coulombic efficiency [5, 9].

The utilization of nanostructured SnO_2 materials was considered as a solution to solve these problems, because it allows to reduce the distance of lithium ion diffusion and increase the number of active sites for reversible reactions [7, 8, 10]. Furthermore, the nano-sized particles assembled with the appropriate architectures can provide a buffer space for volume expansion, allowing to maintain microstructural stability, and limiting the crushing process to break the electrical connections [5, 11]. Currently, the main solutions to be able to prepare high-performance SnO_2-based anode electrodes include: i) Preparation of ultrafine SnO_2 nano-particles to increase specific surface area, reduce mechanical strain, and improve the reversibility of the conversion reaction [11, 12]; ii) Introduction transitional metals or make intermetallic alloys to perform a reversible conversion while minimizing the volume expansion of Sn [13, 14]; and iii) Unique architectural design including surface coating to provide expansion space, preventing full volume expansion [15-18]. In summary, when bare SnO_2 powder is used as the electrode active material, it must be in the nanometer range to shorten the path length of the lithium ion, and there must be hollow space to accommodate the large change in volume.

The aim of this work is to improve the electrochemical performance of the SnO_2 anode electrode materials by using ultrafine SnO_2 nanoparticles prepared by the solvothermal method from $SnCl_4.5H_2O$ precursor. The crystalline structure, morphology, and electrochemical properties of the anode materials for Li-ion battery applications were evaluated and discussed.

2. Experimental

2.1. Preparation of Ultrafine SnO_2 Nano-powder

SnO_2 nano-powder was prepared by solvothermal method using $SnCl_4.5H_2O$ acetate (98%, Sigma–Aldrich) as the initial material. A specific example of the process of preparing SnO_2 superfine nano-powder by solvothermal route is as follows: First, 1.0 g of $SnCl_4.5H_2O$ was dispersed in 80 ml of absolute alcohol for 30 min using a magnetic stirrer and then the solution was further dispersed by

ultrasonication at 30 °C for 30 min. Next, the solution was transferred into a teflon lined autoclave and kept at 180 °C in an oven for 24 h with the heating rate of 10 °C/min, then that was naturally cooled down to room temperature. The resulting products were washed with deionized water and collected by the way of deposition and filtration several times (5-6 times). The collected powders were dried at 50-60 °C overnight and after that, were annealed at 300 °C for 10 min in the air. The rate of increase and decrease of temperature was 10 °C/min. To avoid large agglomeration, the as-annealed powder was ground with an agate pestle and mortar for 30 min. The powder samples were then utilized for their structural and electrochemical characterization.

2.2. Preparation of the Anode Electrode and Test Cell

The working electrode was prepared from a mixture of SnO_2 nano-powder (80 wt. %), black carbon (10 wt. %) as a conductive agent, and polyvinylidene fluoride (PVDF) (10 wt. %) as a binder. The above mixture was mixed together in 99.8% non-aqueous N,N-Dimethylformamide solvent to form a paste which was then casted onto a copper foil with a thickness of 15 μm, and dried at 80 °C in a vacuum oven for 24 h. The test cells (CR2032 coin-type) were assembled in a glove box filled with pure argon gas (99.995%). The relative humidity was controlled at below 5 ppm. Working electrodes were cut from as-prepared SnO_2 electrode plates. Separators were polyethylene membranes. Metallic lithium plates were used as counter and reference electrodes. The electrolyte was a solution of 1M $LiPF_6$ salt in a mixture of ethylene carbonate (EC) and dimethyl carbonate (DEC) solvents with a 1:1 volume ratio.

2.3. Crystalline Structure, Morphology and Electrochemical Characterization

The crystalline structure of the prepared materials was characterized by X-ray diffraction (XRD) with Cu Kα radiation (λ = 1.54056 Å) using an EQUINOX 5000 X-ray diffractometer. The microstructure morphology of the materials was evaluated by field emission scanning electron microscopy (FESEM) "Hitachi S-4800", Japan. The particle size and size distribution were characterized by the particle size analyzer (SZ-100, Horiba Ltd., Japan). The galvanostatic discharge/charge measurements were performed by the Neware BTS-400 battery test system at a current density of 100 $mA \cdot g^{-1}$ in a potential window of 0.01 - 2.5 V. Cyclic voltammetry (CV) at a scanning rate of 0.1 $mV \cdot s^{-1}$ and electrochemical impedance (EI) spectroscopies were investigated by PGSTAT302N AutoLab instrument equipped with AUT86360 module. The collected EI data were analyzed by NOVA software.

3. Results and Discussion

3.1. Crystal Structure and Morphology

The XRD pattern of as-prepared ultrafine SnO_2 powder is shown in Fig. 1. All the diffraction peaks of the (110), (101), (200), (211), (220), (002), (310), (112), (202), (321), (222) and (411) planes could be indexed to the tetragonal rutile structure of SnO_2 in the P42/mnm space group with lattice parameters of a = b = 4.738 Å, c = 3.187 Å (JCPDS Card No. 41–1445). No diffraction peaks from impurities, i.e., other tin oxides, are observed.

It is easy to recognize that the diffraction peaks of the prepared SnO_2 powder are broadened, which proves that the SnO_2 powder has nano-sized crystalline grains. From XRD pattern, the SnO_2 crystalline grain size can be determined using Scherrer's formula. The calculations based on the non-superimposed diffraction peaks revealed that the average crystal grain size of the ultrafine SnO_2 nanoparticles was ca. 7.4 nm.

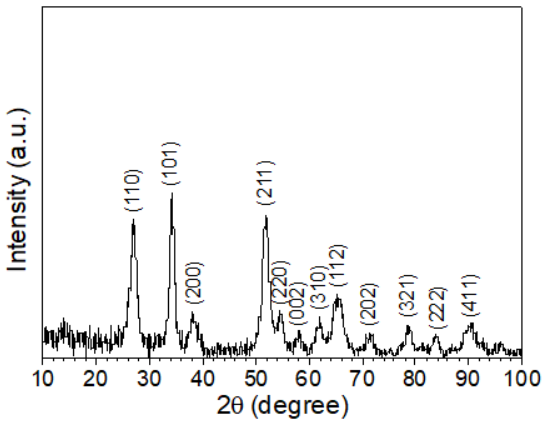

Figure 1. XRD patterns of as-prepared ultrafine SnO_2 nanopowder.

A SEM image of the SnO_2 nanoparticles is displayed in Fig. 2a. As seen, the prepared SnO_2 nanoparticles have spherical shape, quite uniform size in the range of 7-9 nm. SnO_2 nanoparticles tend to agglomerate into larger secondary particles, which are loosely bound together with high porosity. For further information, particle size distribution has been determined by dynamic light scattering technique. As-prepared SnO_2 nanopowder was suspended and ultrasonically vibrated in the ethanol solution. The measured results shown in Fig. 2b indicated that as-prepared SnO_2 nanopowder has narrow size distribution. Their sizes are mostly in the range of 105 to 134 nm with the average value of 119.9 nm. The agglomeration of the nanoparticles seems to be caused by high temperature annealing process.

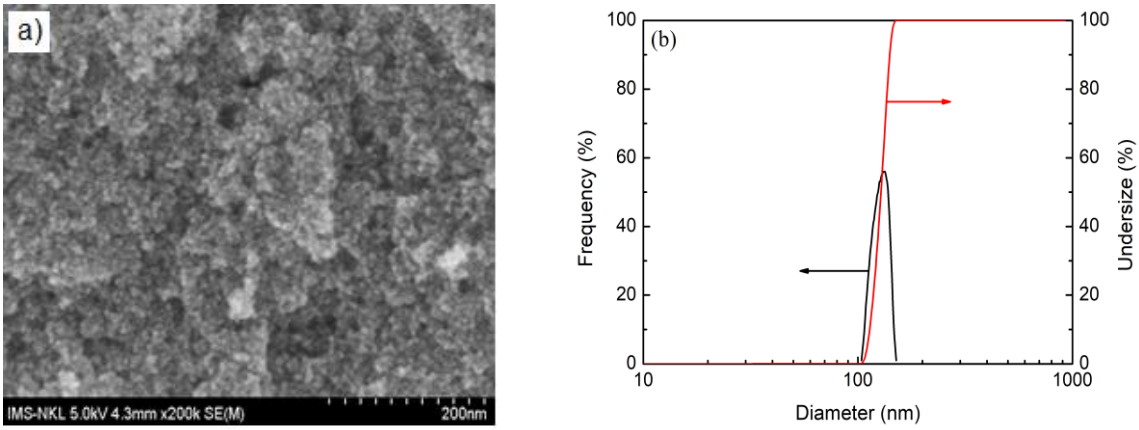

Figure 2. SEM image of the as-prepared SnO_2 nanoparticles (a) and the particle size distribution curve measured by dynamic light scattering technique (b).

3.2. Electrochemical Performances

The electrochemical performance of as-prepared SnO_2 nanoparticles as anode electrode materials for LIB was evaluated by cyclic voltammetry (CV) and galvanostatic discharge - charge cycling tests. The CV measurements were performed to clarify the charge/discharge behavior of the SnO_2 nanoparticles in the range of 0 V - 3.0 V at a scanning rate of 0.1 $mV \cdot s^{-1}$. The redox processes of the

SnO_2 anode in LIB have been extensively studied and generally can be interpreted according to the following equations [12, 19, 20]:

$$Li^+ + e^- + \text{electrolyte} \rightarrow SEI(Li) \quad (1)$$

$$SnO_2 + 2xLi^+ + 2xe^- \leftrightarrow xLi_2O + Sn \quad (2)$$

$$Sn + Li^+ + xe^- \leftrightarrow Li_xSn\ (0 \leq x \leq 4.4) \quad (3)$$

The CV curves of the initial two cycles are shown in Fig. 3a. During the cathodic scanning process, two reduction peaks at 0.77 V and 0.30 V were observed. The broad peak at 0.77 V is attributed to the formation of a solid electrolyte interface (SEI) (reaction 1) and the decomposition of SnO_2 to Sn accompanied by the formation of Li_2O (reaction 2).

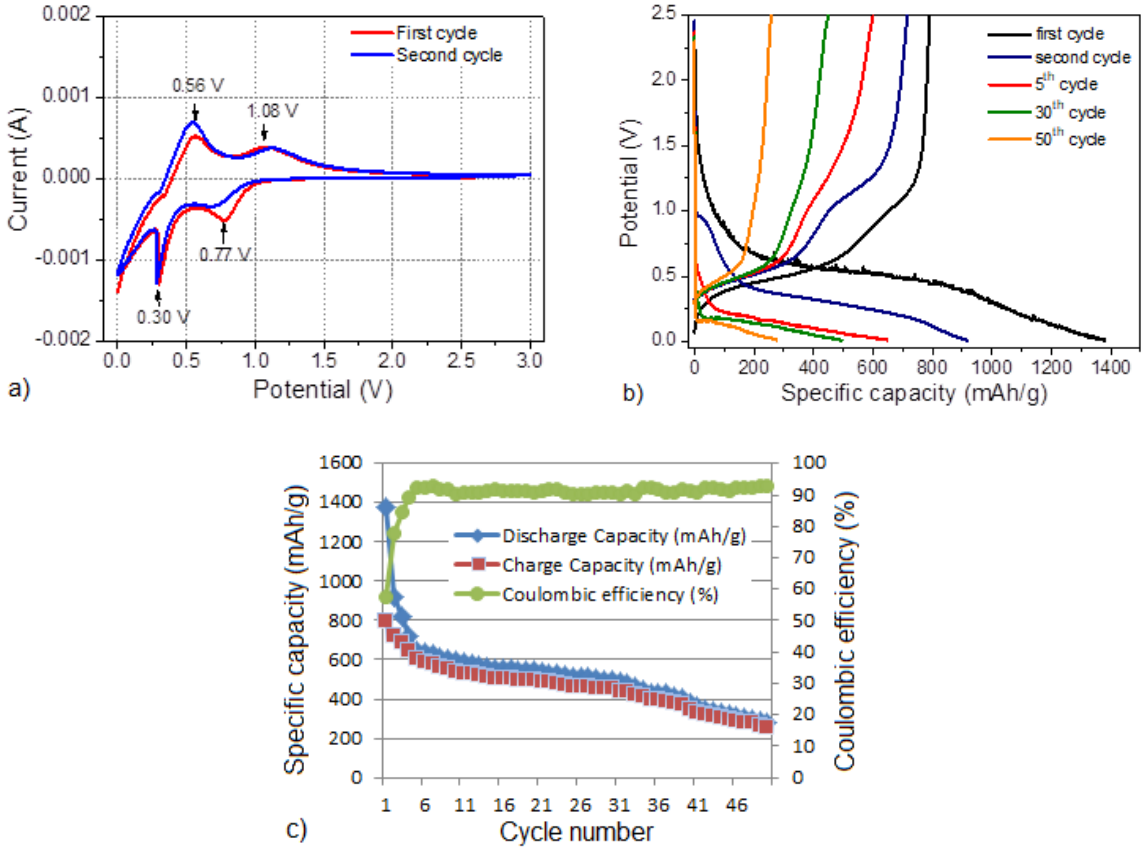

Figure 3. a) Cyclic voltammetry curves of the SnO_2 electrode scanning at the range of 0 - 3.0 V with a scanning rate of $0.1 mV \cdot s^{-1}$; b) Typical discharge-charge curves of SnO_2 electrode at the 1st, 2nd, 5th, 30th, and 50th cycles; c) Cycling performance and Coulombic efficiency vs. cycle number of the SnO_2 electrode at a current density of $100 mA \cdot g^{-1}$.

This reduction peak is often observed to gradually decrease and disappear after several cycles. The reduction peak at 0.30 V can be attributed to the alloying reaction of Li with Sn to form Li_xSn alloy (reaction 3) [12, 19, 20]. During the anodic scanning process, two oxidation peaks at 0.56 V and 1.08 V were observed. The oxidation peak at 0.56 V can be related to the de-alloying process of Li_xSn to Li and Sn. The broad oxidation peak at 1.08 V may correspond to the partially reversible reaction of Li_2O for the formation of SnO_2 (reaction 2) [12, 19-22]. This peak remained stable and could be clearly observed

during subsequently cycles, demonstrating the reversibility of the conversion reactions. The CV curves are almost identical, which shows the high reversibility of the SnO_2 nanoparticle electrode.

The redox behaviors of the SnO_2 electrode can also be revealed from the discharge/charge curves. Figure 3b shows the typical discharge/charge potential curves at a current density of 100 $mAh \cdot g^{-1}$ in a potential window of 0.01 - 2.5 V (versus Li/Li^+). During the first discharge (lithiation) cycle, it was observed that firstly the potential drops rapidly to ~1.5 V, followed by a weakly defined process at a potential of 1.5 – 1.0 V, which can be assigned to the initial decomposition of electrolytes and the formation of solid electrolyte interfaces (SEI) [23]. The voltage plateau at 1.0 V to 0.5 V during the first discharge is attributed to the reduction of SnO_2 to Sn accompanied by the formation of Li_2O (reaction 2). The following long descending plateau was assigned to the Li_xSn alloying formation (reaction 3) [19, 23]. During the first charge (de-lithiation), a plateau-like region of potential at ca. 0.5 V was observed, which corresponds to de-alloying process of Li_xSn to Sn and Li (reaction 3). This was followed by a plateau-like region at ca. 1.1 V corresponding to a partially reversible conversion of Li_2O supported by Sn nanoparticles (reaction 2) [15, 21]. Generally, the redox behaviors observed from the discharge/charge curves are quite similar to those observed from the CV curves. However, it can be found that the oxidation plateau (during charge process) at ca. 1.1 V seems to be disappeared as the number of cycles increased. Since this oxidation region is often assigned to reversible conversion reaction between Li_2O and Sn, the fading of this region can be explained by coarseness of Sn nanoparticles during cycling test. Meanwhile, the fact that oxidation plateau at 0.5 V remained quite stable indicated that the alloying/de-alloying processes are reversible.

Fig. 3c shows the cyclic performance and Coulombic efficiencies of SnO_2 nanoparticle electrode for 50 cycles. The initial charge and discharge specific capacities of the SnO_2 nanoparticles respectively were 792 and 1379 $mAh \cdot g^{-1}$, corresponding to a Coulombic efficiency (CE) of 57%. In the first cycle, the large irreversible capacity loss is mainly due to the decomposition of the electrolyte or some irreversible processes such as the formation of the SEI layer. The low Coulombic efficiency proved that the conversion of Sn to SnO_2 within the charging process was partially reversible [15, 19, 23]. The discharge/charge specific capacities within the second cycle were about 918 $mAh \cdot g^{-1}$ and 716 $mAh \cdot g^{-1}$, respectively, with a Coulombic efficiency of 87%. During the first 5 cycles, the discharge/charge specific capacities decreased quite rapidly, while the Coulombic efficiency gradually increased. The strong capacity loss at this stage is mainly due to the formation of the SEI layer. In addition, severe volume expansion and contraction (up to 300%) during lithium insertion/extraction also play an important role [19]. During the 5^{th} cycle, the specific discharge/charge capacities were reduced to ~648 $mAh \cdot g^{-1}$ and ~600 $mAh \cdot g^{-1}$, and the Coulombic efficiency reached ~93%. After the 5^{th} cycle, the Coulombic efficiency was almost constant (about 91-93%), while the discharge/charge specific capacities continued to decrease gradually as the number of cycles increased. From the 5^{th} to the 30^{th} cycles, the rate of capacity loss was estimated to be ~1%/cycle, and increasing to ~2%/cycle from the 30^{th} to the 50^{th} cycles. The discharge/charge specific capacities after 50^{th} cycles remained at ~276 $mAh \cdot g^{-1}$ and ~258 $mAh \cdot g^{-1}$, respectively. The rapid decrease in specific capacity during this stage was caused mainly by the electrode pulverization which resulted from the large volume expansion/contraction during the lithiation/delithiation processes [21]. In fact, after the 50^{th} cycle, the capacity loss increased abruptly (not shown here).

3.3. Electrochemical Impedance

The electrochemical impedance spectra of the Li/SnO_2 half-cell before and after cycling test are shown in Fig. 4a and Fig. 4b, respectively. Typical feature of the Nyquist plots includes a compressed semicircle at high frequency range and a slanting straight line at low frequency range. The compressed semicircle is the result of the overlap of two semicircles: one representing the SEI and the other

representing the charge transfer in the active material of the electrode [19, 21, 24]. The intercept of the semicircle with the Z' axis towards the high frequency corresponds to the bulk resistance value (R_b) which is the resistance of the electrolyte, the separator and the current collector [25]. The diameter of the semicircle represents the sum of the solid-electrolyte interface resistance (R_{SEI}) and charge transfer resistance (R_{ct}) at the electrode/electrolyte interfaces. The slanting straight line represents the Warburg impedance (W), which is related to the diffusion of lithium ions in the active material. The resistances of R_b and R_{SEI} + R_{ct} can be determined by the intercept points of the semicircle with the Z' axis [19, 25].

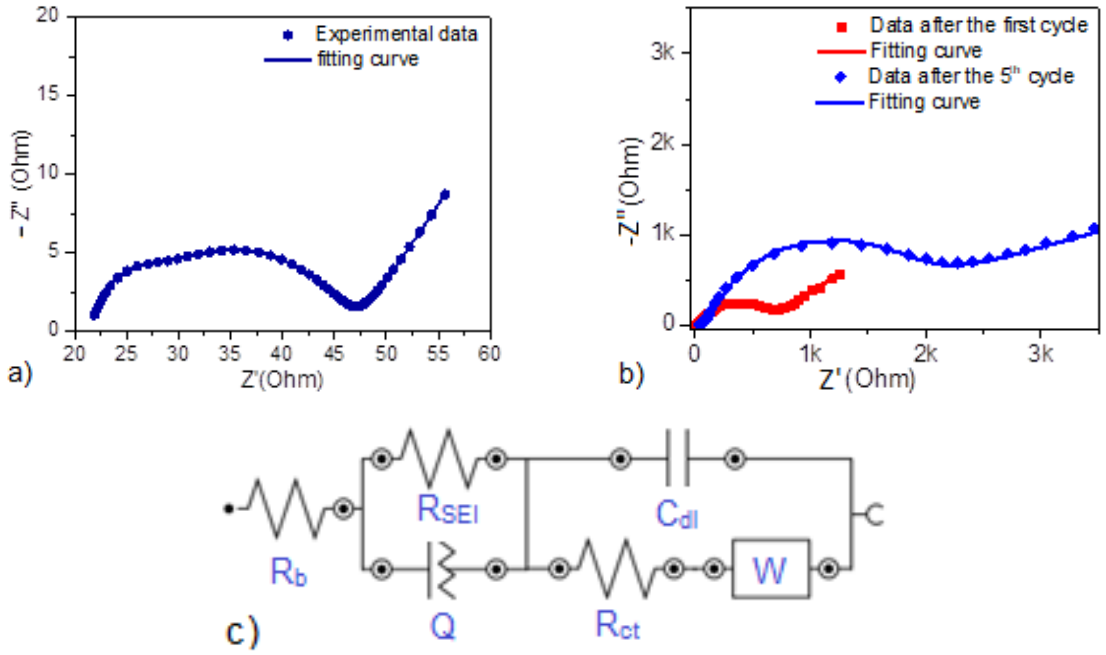

Figure 4. Nyquist plots of the Li/SnO_2 half-cells obtained before the cycle (a) and after the first and fifth discharge/charge cycles (b); c) Equivalent circuit model of Li/SnO_2 half-cell.

In order to determine more precisely and to be able to separate the resistances R_b, R_{EIS} and R_{ct} of the SnO_2 electrode, the fitting method of the curve obtained from an equivalent circuit to the experimental data spectrum was used. The equivalent circuit model used for the fit is shown in Fig. 4c. Here, R_b is bulk resistance; R_{SEI} and Q are resistance and constant phase element of the SEI, respectively; R_{ct} and C_{dl} are a charge-transfer resistance and double-layer capacitance, respectively; W is the Warburg impedance [25]. It is found that the curves obtained from the equivalent circuit fitted well with the experimental spectra (Fig. 4a, b). According to this equivalent circuit (Fig. 4c), the fitted impedance values are shown in Table 1.

Table 1. The fitted results of impedance spectra for the SnO_2 cell at different stages

Stage	R_b (Ω)	R_{SEI} (Ω)	Q		R_{ct} (Ω)	W (mMho)	C (μF)
			Y_0 (μMho)	n			
Before cycling	21.2	22.6	224	0.532	3.33	103	0.544
After first cycle	12.6	388	163	0.509	299	1.59	9.47
After 5th cycle	25.4	660	522	0.364	1459	1.29	9.05

Firstly, it was found that the bulk resistance did not change much with the number of cycles. It decreased initially because the current collector-electrode and electrode-electrolyte contacts got better over some initial discharge/charge cycles. But as cycling continues, it gradually increased due to the electrolyte depletion, binder decomposition, corrosion of the current collector and the formation of micro-cracks in the particles which lead to performance degradation of electrode [25]. Secondly, SEI is formed on the electrode-electrolyte interface, immediately after the half-cell is assembled due to electrolyte decomposition and conversion reaction [4, 24, 25]. The increase of R_{SEI} resistance with increasing cycle indicated that although the reversible conversion reaction occurs (as analyzed in section 3.2), it was only partial. Thirdly, the rapid increase of charge transfer resistance R_{ct} with the number of cycles was attributed to the agglomeration and pulverization of the active material that led to a decrease in the active zone and loss of the electrical contacts [15, 25].

4. Conclusion

In summary, ultrafine SnO_2 nanoparticles with an average crystal grain size of 7.4 nm have been successfully prepared by a facile solvothermal route. SnO_2 nanoparticles are cassiterite type belonging to tetragonal crystal system with rutile structure, with good dispersibility. The results of the electrochemical measurements show that as-prepared ultrafine SnO_2 nanoparticles have large charge/discharge specific capacities, but its cyclic stability is relatively low. To be usable as an anode material for next-generation Li-ion batteries, the strategies allow for reduction of the large volume expansion causing the loss of electrical contact, agglomeration, and formation of coarse Sn particles that reduce the reversibility of the conversion during lithium insertion/extraction need to be further investigated in more detail.

Acknowledgement

This work is supported by the Science & Technology Project (2019-2021) from Ministry of Education and Training (Project code: B2019-SP2-06).

References

[1] V. Etacheri, R. Marom, R. Elazari, G. Salitra, D. Aurbach, Challenges in the Development of Advanced Li-ion Batteries: A Review, Energy Environ.Sci., No. 4, 2011, pp. 3243-3262, https://doi.org/10.1039/C1EE01598B.

[2] N. Nitta, F. Wu, J. T. Lee, G. Yushin, Li-ion Battery Materials: Present and Future, Mater. Today, Vol. 18, No. 5, 2015, pp. 252-264, https://doi.org/10.1016/j.mattod.2014.10.040.

[3] J. M. Tarascon, M. Armand, Issues and Challenges Facing Rechargeable Lithium Batteries, Nature, Vol. 414, 2001, pp. 359-367, https://doi.org/10.1142/9789814317665_0024.

[4] W. W. Lee, J. M. Lee, Novel Synthesis of High Performance Anode Materials for Lithium-ion Batteries (LIBs), J. Mater. Chem. A, Vol. 2, 2014, pp. 1589-1626, https://doi.org/10.1039/C3TA12830J.

[5] L. Liu, F. Xie, J. Lyu, T. Zhao, T. Li, B. G. Choi, Tin-based Anode Materials with Well-designed Architectures for Next-generation Lithium-ion Batteries, Journal of Power Sources, Vol. 321, 2016, pp. 11-35, https://doi.org/10.1016/j.jpowsour.2016.04.105.

[6] A. R. Kamali, D. J. Fray, Tin-based Materials as Advanced Anode Materials for Lithium Ion Batteries: A Review, Rev. Adv. Mater. Sci, Vol. 27, 2011, pp. 14-24.

[7] R. Mukherjee, R. Krishnan, T. M. Lu, N. Koratkar, Nanostructured Electrodes for High-power Lithium Ion Batteries, Nano Energy, Vol. 1, No. 4, 2012, pp. 518-533, https://doi.org/10.1016/j.nanoen.2012.04.001.

[8] K. T. Lee, J. Cho, Roles of Nanosize in Lithium Reactive Nanomaterials for Lithium Ion Batteries, Nano Today, Vol. 6, No. 1, 2011, pp. 28-41, https://doi.org/10.1016/j.nantod.2010.11.002.

[9] L. Chang, Z. Yi, Z. Wang, L. Wang, Y. Cheng, Ultrathin SnO_2 Nanosheets Anchored on Graphene with Improved Electrochemical Kinetics for Reversible Lithium and Sodium Storage, Applied Surface Science, Vol. 484, 2019, pp. 646-654, https://doi.org/10.1016/j.apsusc.2019.04.144.

[10] P. Jajarmi, S. Barzegar, G. R. Ebrahimi, N. Varahram, Production of SnO_2 Nano-particles by Hydrogel Thermal Decomposition Method, Materials Letters, Vol. 65, No. 9, 2011, pp. 1249-1251, https://doi.org/10.1016/j.matlet.2010.10.028.

[11] Y. Wang, H. Li, P. He, E. Hosono, H. Zhou, Nano Active Materials for Lithium-ion Batteries, Nanoscale, Vol. 2, 2010, pp. 1294-1305, https://doi.org/10.1039/c0nr00068j.

[12] P. Deng, J. Yang, S. Li, T. E. Fan, H. H. Wu, Y. Mou, H. Huang, Q. Zhang, D. L. Peng, B. Qu, High Initial Reversible Capacity and Long Life of Ternary SnO_2-Co-carbon Nanocomposite Anodes for Lithium-Ion Batteries, Nano-Micro Lett., Vol. 11, No. 18, 2019, https://doi.org/10.1007/s40820-019-0246-4.

[13] Y. Deng, C. Fang, G. Chen, The Developments of SnO_2/Graphene Nanocomposites as Anode Materials for High Performance Lithium ion Batteries: A Review, Journal of Power Sources, Vol. 304, 2016, pp. 81-101, https://doi.org/10.1016/j.jpowsour.2015.11.017.

[14] L. Zu, Q. Su, F. Zhu, B. Chen, H. Lu, C. Peng, T. He, G. Du, P. He, K. Chen, S. Yang, J. Yang, H. Peng, Antipulverization Electrode Based on Low-Carbon Triple-Shelled Superstructures for Lithium-Ion Batteries, Adv. Mater., Vol. 29, No. 34, 2017, pp. 1701494, https://doi.org/10.1002/adma.201701494

[15] R. Hu, H. Zhang, Z. Lu, J. Liu, M. Zeng, L. Yang, B. Yuan, M. Zhu, Unveiling Critical Size of Coarsened Sn Nanograins for Achieving High Round-Trip Efficiency of Reversible Conversion Reaction in Lithiated SnO_2 Nanocrystals, Nano Energy, Vol. 45, 2018, pp. 255-265. https://doi.org/10.1016/j.nanoen.2018.01.007

[16] Q. Zhao, Y. Xie, T. Dong, Z. Zhang, Oxidation-Crystallization Process of Colloids: An Effective Approach for the Morphology Controllable Synthesis of SnO_2 Hollow Spheres and Rod Bundles, J. Phys. Chem. C, Vol. 111, No. 31, 2007, pp. 11598-11603, https://doi.org/10.1021/jp072858h.

[17] S. Han, B. Jang, T. Kim, S. M. Oh, T. Hyeon, Simple Synthesis of Hollow Tin Dioxide Microspheres and Their Application to Lithium-ion Battery Anodes, Adv. Funct. Mater, Vol. 15, No. 11, 2005, pp. 1845-1850, https://doi.org/10.1002/adfm.200500243.

[18] Q. He, J. Liu, Z. Li, Q. Li, L. Xu, B. Zhang, J. Meng, Y. Wu, L. Mai, Solvent-free Synthesis of Uniform MOF Shell-Derived Carbon Confined SnO_2/Co Nanocubes for Highly Reversible Lithium Storage. Small, Vol. 13, No. 37, 2017, pp. 1701504, https://doi.org/10.1002/smll.201701504.

[19] L. Yin, S. Chai, F. Wang, J. Huang, J. Li, C. Liu, X. Kong, Ultrafine SnO_2 Nanoparticles as a High Performance Anode Material for Lithium Ion Battery, Ceramics International, Vol. 42, No. 8, 2016, pp. 9433-9437, https://doi.org/10.1016/j.ceramint.2016.02.173.

[20] S. Zhou, H. Zhou, Y. Zhang, K. Zhu, Y. Zhai, D. Wei, S. Zeng, SnO_2 Anchored in S and N Co-Doped Carbon as the Anode for Long-Life Lithium-Ion Batteries, Nanomaterials, Vol. 12, No. 4, 2022, pp. 700, https://doi.org/10.3390/nano12040700.

[21] L. Feng, Z. Xuan, S. Ji, W. Min, H. Zhao, H. Gao, Preparation of SnO_2 Nanoparticle and Performance as Lithium-ion Battery Anode, Int. J. Electrochem. Sci., Vol. 10, 2015, pp. 2370-2376.

[22] X. Zhou, L. Yu, X. W. D. Lou, Formation of Uniform N-doped Carbon-Coated SnO_2 Submicroboxes with Enhanced Lithium Storage Properties, Adv. Energy Mater. Vol. 6, No. 14, 2016, pp. 1600451, https://doi.org/10.1002/aenm.201600451.

[23] R. S. Periathai, R. P. Vengatesh, N. Jeyakumaran, N. Prithivikumaran, Investigation on Synthesis of SnO_2 Nano-particles Using Sol–Gel Process for Energy Storage Application, Australian Journal of Electrical and Electronics Engineering, Vol. 17, No. 2, 2020, pp. 114-121, https://doi.org/10.1080/1448837X.2020.1786294.

[24] X. Y. Liu, Y. L Han, Q. Li, D. Pan, SnO_2 Nanoparticles for Lithium-Ion Batteries Prepared by Sol-Gel Method, Key Engineering Materials, Vol. 727, 2017, pp. 718-725, zhttps://doi.org/10.4028/www.scientific.net/KEM.727.718.

[25] W. Choi, H. C. Shin, J. M. Kim, J. Y. Choi, W. S. Yoon, Modeling and Applications of Electrochemical Impedance Spectroscopy (EIS) for Lithium-ion Batteries, J. Electrochem. Sci. Technol. Vol. 11, No. 1, 2020, pp. 1-13, https://doi.org/10.33961/jecst.2019.00528.